Cancer Letters 364 (2015) 142–155

Contents lists available at ScienceDirect

Cancer Letters

journal homepage: www.elsevier.com/locate/canlet

Original Articles

The development of cisplatin resistance in neuroblastoma is accompanied by epithelial to mesenchymal transition *in vitro*

Olga Piskareva [a,b,*], Harry Harvey [a,b], John Nolan [a,b], Ross Conlon [a,b], Leah Alcock [a], Patrick Buckley [c], Paul Dowling [d,e], Michael Henry [e], Finbarr O'Sullivan [e], Isabella Bray [a,b], Raymond L. Stallings [a,b]

[a] *Cancer Genetics Group, Department of Molecular and Cellular Therapeutics, Royal College of Surgeons in Ireland, Dublin 2, Ireland*
[b] *Children's Research Centre, Our Lady's Children's Hospital, Crumlin, Dublin 12, Ireland*
[c] *Molecular Pathology Laboratory, Beaumont Hospital, Dublin 9, Ireland*
[d] *Department of Biology, The National University of Ireland Maynooth, Maynooth, County Kildare, Ireland*
[e] *National Institute for Cellular Biotechnology, Dublin City University, Dublin 9, Ireland*

ARTICLE INFO

Article history:
Received 18 February 2015
Received in revised form 10 April 2015
Accepted 4 May 2015

Keywords:
Neuroblastoma
Proteomics
Cisplatin
Drug resistance
Epithelial-to-mesenchymal transition (EMT)
Invasion

ABSTRACT

Neuroblastoma is a challenging childhood malignancy, with a very high percentage of patients relapsing following acquisition of drug resistance, thereby necessitating the identification of mechanisms of drug resistance as well as new biological targets contributing to the aggressive pathogenicity of the disease. In order to investigate the molecular pathways that are involved with drug resistance in neuroblastoma, we have developed and characterised cisplatin resistant sublines SK-N-ASCis24, KellyCis83 and CHP-212Cis100, integrating data of cell behaviour, cytotoxicity, genomic alterations and modulation of protein expression. All three cisplatin resistant cell lines demonstrated cross resistance to temozolomide, etoposide and irinotecan, all of which are drugs in re-initiation therapy. Array CGH analysis indicated that resistant lines have acquired additional genomic imbalances. Differentially expressed proteins were identified by mass spectrometry and classified by bioinformatics tools according to their molecular and cellular functions and their involvement into biological pathways. Significant changes in the expression of proteins involved with pathways such as actin cytoskeletal signalling ($p = 9.28E{-}10$), integrin linked kinase (ILK) signalling ($p = 4.01E{-}8$), epithelial adherens junctions signalling ($p = 5.49E{-}8$) and remodelling of epithelial adherens junctions ($p = 5.87E{-}8$) pointed towards a mesenchymal phenotype developed by cisplatin resistant SK-N-ASCis24. Western blotting and confocal microscopy of MYH9, ACTN4 and ROCK1 coupled with invasion assays provide evidence that elevated levels of MYH9 and ACTN4 and reduced levels of ROCK1 contribute to the increased ROCK1-independent migratory potential of SK-N-ASCis24. Therefore, our results suggest that epithelial-to-mesenchymal transition is a feature during the development of drug resistance in neuroblastoma.

Introduction

Neuroblastoma, a paediatric cancer of the sympathetic nervous system, is characterised by a highly heterogeneous clinical behaviour, ranging from spontaneous regression to rapid progression and patient death [1]. The clinical course depends on the molecular characteristics of the tumor, patient age, disease stage, and states of differentiation. Patients with high risk disease (tumours with either *MYCN* amplification or deletions on the long arm of chromosome 11, large numbers of segmental chromosomal imbalances, stage 4 disease) still have relatively low overall survival rates (~40%) in spite of intensive multimodal chemotherapy. The initial induction chemotherapy often includes a combination of cisplatin, vincristine, carboplatin, etoposide and cyclophosphamide. Surgery, radiation and myeloablative treatments using escalating chemotherapeutic combinations followed by bone marrow infusion are also used on high-risk cases. Post-initiation treatment patients are routinely prescribed 13-*cis*-retinoic acid (RA) as a maintenance therapy for 6 months and immunotherapy with the chimeric anti-GD2 antibody ch14.18, both of which have led to improved event free survival [2]. Nevertheless, the 5 year survival rate is only ~15% for patients with relapse disease who were originally diagnosed with high risk neuroblastoma, in spite of treatment with additional drugs such as topotecan and temozolomide [3], presumably due to the development of multi-drug resistance.

Relapse disease with the emergence of drug resistant tumour cells is a major impediment to the successful treatment of high risk neuroblastoma patients. The development of drug resistance

* Corresponding author. Tel: +353 1 4022123; fax: +353 1 4202453.
E-mail address: olgapiskareva@rcsi.ie (O. Piskareva).

http://dx.doi.org/10.1016/j.canlet.2015.05.004

involves the acquisition of multiple genetic and epigenetic changes leading to aberrant RNA and protein expression. These changes affect many pathways, including those that alter the cytoskeleton, copper metabolism, cell surface presentation of proteins and epithelial-to-mesenchymal transition (EMT). It is not surprising therefore that several mechanisms mediating chemotherapeutic resistance have been identified, including decreased drug uptake by the solute carrier family of transporters, increased drug efflux from cells by the adenosine triphosphate-binding cassette family of membrane transport proteins, gain in DNA damage repair mechanisms and failure of the cell death pathways (detailed in [4]).

Acquired or innate resistance to chemotherapeutic agents is the single most important factor leading to therapy failure and recurrence of malignant disease. Thus, the identification of new biological targets that facilitate early diagnosis and/or contribute to the aggressive pathogenicity of this disease, along with the development of reagents that will interfere with the function of these targets, is a prerequisite for improving patient survival.

In order to identify further molecular pathways that are involved with drug resistance in neuroblastoma, we have developed cisplatin resistant sublines of SK-N-AS, Kelly and CHP-212 cell lines. Cisplatin activates apoptosis by forming DNA intrastrand cross-links known as platinum-DNA adducts [4]. Cisplatin acts on several signalling pathways, triggering mechanisms that are involved in resistance development by establishing a complicated self-defence system to escape exogenous cytotoxic compounds of different origins. In the work presented here, we report proteomic profiling of each of these drug resistant lines and their respective drug sensitive parental line. The SK-N-AS resistant subline, SK-N-ASCis24, was shown to have increased resistance to apoptosis through increased expression of the neuronal apoptosis inhibitory protein (NAIP) gene through a combination of DNA copy number gain and reduced miRNA signalling [5]. Here, we show through proteomic profiling and functional studies that the SK-N-ASCis24 variant has undergone an epithelial-to-mesenchymal transition in addition to acquiring a drug resistant phenotype.

Materials and methods

Cell culture and transfections

CHP-212 is a *MYCN* amplified cell line derived from a kidney mass from a 20 month old male infant whose INSS disease stage is unknown. The Kelly cell line is a *MYCN* amplified cell line with a 17q chromosomal gain. The SK-N-AS cell line is a *MYCN* diploid cell line derived from the metastatic bone marrow mass of INSS stage 4 disease of an 8 year old female. It has a deletion at chromosome 1p and 11q as well as a gain at 17q.

CHP-212, Kelly and SK-N-AS cell lines were obtained from the European Cell Culture Collection. CHP-212 cells were cultured in a 1:1 mixture of Eagle's Minimum Essential Medium (Gibco, #21090-022) and Ham's F12 Medium (Gibco, #21765-029), 1% Non-essential Amino Acids (Gibco, #11140-050), 200 mM Glutamine (Gibco, #25030-024), 10% Foetal Bovine Serum (Gibco, #10270106), 1% Penicillin/Streptomycin (Gibco, #15070). Kelly cells were cultured in RPMI (Gibco, #21875-034), 10% Foetal Bovine Serum (Gibco, # 10270106), 1% Penicillin/Streptomycin (Gibco, #15070). SK-N-AS cells were cultured in MEM (Gibco, #21090-022), 1% Non-essential Amino Acids (Gibco, #11140-050), 200 mM Glutamine (Gibco, #25030-024), 10% Foetal Bovine Serum (Gibco, #10270106), 1% Penicillin/Streptomycin (Gibco, #15070). All cell lines were incubated at 37 °C in a humidified chamber with 5% CO_2. The chemotherapy resistant sub-lines were selected by exposing cells to increasing concentrations of cisplatin over a 6 month period as described previously for SK-N-AS [5]. Cells were routinely screened for mycoplasma using MycoAlert Mycoplasma Detection kit (Lonza, #LT07-318). Cell lines were authenticated by STR PCR (SOP ECACC/047).

MTT assay

Cells were seeded at 1×10^4 cells/mL suspension in 96-well plates at 100 µL/well and incubated overnight at 37 °C in 5% CO_2. The following cytotoxic drugs were used in this study: Cisplatin (Hospira UK, #PA437/4/7), Etoposide (Ebewe Pharma, #pa789/13/1), Temozolomide (Sigma-Aldrich, #T2577) and Irinotecan (Sigma-Aldrich, #I1406). Cytotoxic drug was added in a serial dilution and cell growth was monitored over 5–7 days. Assessment of cell viability was determined using an acid phosphatase assay as previously described [5].

Array comparative genomic hybridisation

aCGH was carried out as previously described [6] using a 72,000 feature array (NimbleGen).

Cell lysis

Preparations of cell lysates for proteomic analysis were repeated in identical conditions of cell growth. Cells were harvested when they reached a 75–80% confluence in T75 culture flasks in complete media.

The cell pellet was resuspended in lysis buffer (50 mM Tris, pH 8, 150 mM NaCl, 2% NP-40, 0.5% sodium deoxycholate and 0.1% SDS). Lysis of cells was also aided by three freeze–thaw cycles in liquid nitrogen. Protein lysates were clarified by centrifugation (16,000 × g, 40 min, 4 °C). Protein concentration was determined by Coomassie (Bradford) Protein Assay Kit (Pierce, # 23200).

Mass spectrometry

Digested samples were resuspended in 0.1% TFA in 2% ACN (Fluka, #34976-2.5L-R) and analysed by nanoLC-MS/MS using an Ultimate 3000 system (Dionex) coupled to a nanospray LTQ Orbitrap mass spectrometer (Thermo Fisher Scientific), using a linear ACN gradient from 0% to 65% CAN (Sigma, #84378-1L) over 180 min. Buffers used for nano-LC separation contained 0.1% formic acid as the ion pairing reagent. The flow rate was 300 nL/min. The LTQ Orbitrap was operated in data-dependent acquisition mode with Xcalibur software. Survey scan MS data were acquired in the Orbitrap on the 300–2000 m/z mass range with the resolution set to a value of 60,000 at 400 m/z. The five most intense ions per survey scan were selected for MS/MS fragmentation and the resulting fragments were analysed in the linear trap. Collision energy was set to 35%. Dynamic exclusion was employed within 60 s. Full scan mass spectra were recorded in profile mode and tandem mass spectra in centroid mode. Biological replicates (n = 3) were analysed for each sample type.

Progenesis analysis

RAW files were analysed in Progenesis LC-MS software. This software extracts quantitative information from MS1 data by aligning each LC–MS run to a reference file. The results were filtered based on statistical analysis. Any peptides with an ANOVA score of $p > 0.05$ were eliminated. The MS2 data for the remaining peptides were exported and the resulting MGF file was used to search the Swissprot database (Release 2011_05) on the MASCOT server (www.matrixscience.com) for protein identifications. The Mascot parameters were (1) species, Homo sapiens, (2) allowed number of missed cleavages, 1, (3) fixed modification, carboxylmethyl, (4) variable modifications, methionine oxidation (5) peptide tolerance, ± 20 ppm, (6) MS/MS tolerance, ± 0.6 Da and (7) peptide charge, + 2, +3 and +4. Peptides were also searched against a decoy database to determine the false discovery rate (FDR).

The total number of statistically significant peptides/features (p value ≤0.05) exported to Mascot for database searching was 877 (KellyCis83 versus Kelly), 1366 (SK-N-ASCis24 versus SK-N-AS), and 1642 (CHP-212Cis100 versus CHP-212). Based on these, a total of 118, 97 and 111 proteins (p value ≤0.05, a fold change ≥1.2, FDR ≤1% and Mascot score>40) were identified respectively. Peptide conflicts were resolved by assigning the peptide to the protein with the greater number of hits, a greater Mascot score or a lower mass error; when conflicts could not be clearly resolved, the peptide was excluded from the analysis.

Immunodetection

Total protein was analysed by western blotting using primary antibodies anti-ACTN4 (Abcam, #ab32816), anti-MYL12B (Abcam, #ab137063), anti-MYH9 (Abcam, #ab55456), anti-alpha-tubulin (Abcam, #ab7291), anti-beta-actin (Abcam, #ab6276), anti-VIM (Cell Signaling Technology, #3295), Anti-Zeb1-[Anti-AREB6 antibody [3G6]-N-terminal] (Abcam, #ab180905), Anti-Twist antibody [Twist2C1a] (Abcam, #ab50887), and Anti-SNAIL antibody (Abcam, #ab180714), followed by anti-mouse (Abcam, #ab6728) or anti-rabbit (Abcam, #ab97200) secondary antibody. Immunofluorescence staining was visualised using DAPI (Invitrogen, #D1306), anti-mouse Alexa Flour®647 (Invitrogen, #A-21239) and anti-rabbit Alexa Flour®488 (Invitrogen, #A-11034) secondary antibody using a Leica SP2 AOBS confocal microscope. Subsequent image processing was conducted using AutoquantX and Metamorph.

Invasion assay

The 8 µm pore size PET BD BioCoatTM Growth Factor Reduced (GFR) MATRIGEL Invasion Chambers (BD Biosciences, #354481) were used as per manufacturer's instruction. Kelly cells were seeded at 10^5 cells per chamber while CHP-212 and SK-N-AS cells were seeded at 0.5×10^5 cells per chamber. Briefly, cell suspensions in serum free culture media were added into the upper chamber of the insert. The bottom chamber contained culture media containing 10% FBS. After a 48 hr incubation at 37 °C, 5% CO_2 atmosphere, non-invading cells were removed, the inner side of the insert was washed with PBS and the outer side was stained with 0.25% crystal violet for 10 min. Inserts were then viewed under the microscope. Invading cells were

counted by taking ten images at random points and manually counting cells, the average of the ten images was then calculated.

Bioinformatics analysis

Bioinformatics analysis and annotations of the proteins identified were carried out based on their biological functions and cellular localisations as per Human Protein Reference Database (http://www.hprd.org), which is in compliance with Gene Ontology standards.

Ingenuity Pathway Analysis (IPA, Ingenuity® Systems) was performed to outline the most significant canonical pathways and functions in the datasets. Detailed methods for this procedure have been described previously [63].

In brief, identifiers from the datasets were uploaded into IPA and these were mapped to the corresponding genes. These genes were overlaid onto the global molecular network developed from information contained in the Ingenuity Pathways Knowledge Base. Networks of the genes in the dataset were then algorithmically generated based on their connectivity. These networks were scored based on the number of molecules included in the networks, with the score corresponding to the negative logarithm of the p-value corresponding to the presence of these molecules in the network by chance. The significance of the association between the dataset and the canonical pathway was measured in two ways: (1) the ratio of the number of genes from the dataset that map to a given canonical pathway was divided by the total number of genes that map to the same canonical pathway; and (2) Fisher's exact test was used to calculate a P-value to determine the probability that the association between the genes in the dataset and the canonical pathway could be explained by chance alone. After the datasets were uploaded, each gene identifier was mapped to its corresponding gene object in the IPA Knowledge Base, and these genes were overlaid onto a global molecular network. Gene networks were then algorithmically generated based on their connectivity.

Statistics

All statistical analysis was performed using GraphPad Prism 5 software (GraphPad Software). The IC50 values were calculated by a non-linear least squares regression model to fit the data to the log (inhibitor) versus response (variable slope). Statistical significance was assessed for a shift in IC50 of resistant cell line compared to the parental using an actual dose of the drug nearest to the calculated IC50.

Statistical significance was determined for all experimental data by using the unpaired Student's t-test. In all cases error bars are representative of the standard deviation of the mean of three biological experiments unless otherwise stated. A P-value of <0.05 was regarded as statistically significant (* $p < 0.05$; ** $P < 0.01$; *** $P < 0.001$).

Results

In order to identify the genetic pathways mediating drug resistance in neuroblastoma, we developed and characterised 3 pairs of sensitive and drug resistant neuroblastoma cell lines, integrating data of cell behaviour, genomic alterations and modulation of protein expression.

Establishment and characterisation of cisplatin resistant CHP-212, Kelly and SK-N-AS cell lines

The cisplatin resistant subline of SK-N-AS, SK-N-ASCis24, has recently been described by Harvey et al. [5], and using similar methods of pulse exposure to increasing concentrations of cisplatin over a period of six months, cisplatin resistant sublines for Kelly (KellyCis83) and CHP-212 (CHP-212Cis100) were also developed. Initial dose for all cell lines was 2 μM. Maximum doses for SK-N-AS, Kelly and CHP-212 were 24 μM, 83 μM and 100 μM, respectively. The half maximal inhibitory concentration (IC50) values of the six cell lines are summarised in Table 1. A higher final concentration for pulse selection was necessary for CHP-212, as parental cells have a high intrinsic resistance to cisplatin in comparison to SK-N-AS and Kelly cells. As summarised in Table 1, each of the cisplatin resistant sublines exhibited cross resistance to a number of other drugs used in the neuroblastoma treatment regimen, including etoposide and irinotecan. No significant cross resistance was detected to temozolomide. Differences in cell morphology were also observed between cisplatin resistant and parental cells by phase contrast microscopy (Fig. 1A). This was most notable for SK-N-ASCis24 cells, which became more elongated in comparison with the polygonal morphology of the parental cell line. Array CGH analysis indicated that all of the resistant lines have acquired additional genomic imbalances (Supplementary File S1). The doubling time of drug resistant cells differed from the parental lines, increasing for SK-N-ASCis24 and CHP-212Cis100 from 33 hrs to 74 hrs and from 48 hrs to 70 hrs, respectively, while decreasing for KellyCis83 from 51 to 33 hrs. A significant increase in the invasive ability was observed for CHP-212Cis100 (2.8-fold change) and SK-N-ASCis24 (2.5-fold change) (Fig. 1D). No significant change in the invasiveness of KellyCis83 was detected.

Proteomic profiling of cisplatin sensitive and resistant human neuroblastoma cells

Comparative proteomic analysis using label free mass spectrometry was carried out on each parental and drug resistant cell line in triplicate. A total of 111 significant ($p \leq 0.05$, fold change ≥ 1.2) protein expression changes were registered in the CHP-212Cis100 resistant cell line, 118 in KellyCis83, and 97 in SK-N-ASCis24 (Fig. 1B), when compared to their sensitive parental lines. More proteins were up-regulated than down-regulated in CHP-212Cis100 relative to parental cells, whereas the opposite occurred in KellyCis83 and SK-N-ASCis24 (Fig. 2C). A full list of protein abundance changes detected for each cell line as well as MS data are available in Supplementary File S2. Out of a total 326 identified proteins, 73 were differentially expressed in two out of three datasets, 35 of which were differentially expressed in the same direction in at least two drug resistant cell lines (Table 2). Only B-tubulin (TUBB) was differentially expressed in all three cell lines in the same direction (under-expressed).

Classification of modulated proteins in cisplatin-sensitive and resistant neuroblastoma cell lines by ingenuity pathway analysis

To answer the question of whether the development of cisplatin resistance involves similar type of proteins, we used Ingenuity Pathway Analysis software (IPA) to analyse the differentially expressed proteins for each individual cell line pair. The analysis for 'molecular and cellular functions' indicated that the top scoring function was cellular growth and proliferation, followed by cell death and survival (Fig. 2A and Table 3), both consistent with

Table 1
IC50 values of six cell lines. The value of IC50 of the sensitive and resistant cells to the tested drugs.

Cell line	Cisplatin	Fold resistance	p value	Etoposide	Fold resistance	p value	Irinotecan	Fold resistance	p value	Temozolomide	Fold resistance	p value
Kelly	1.40 ± 0.25	1		0.12 ± 0.01	1		0.18 ± 0.02	1		139.20 ± 5.95	1	
KellyCis83	2.45 ± 0.40	1.75	0.0001	0.16 ± 0.02	1.33	0.004	0.37 ± 0.04	2.0	0.002	251.00 ± 15.75	1.80	0.09
SK-N-AS	0.68 ± 0.09	1		0.24 ± 0.03	1		0.82 ± 0.07	1		227.70 ± 22.15	1	
SK-N-ASCis24	3.60 ± 0.57	5.3	0.00002	0.57 ± 0.11	2.25	0.004	4.40 ± 0.98	5.37	0.007	480.60 ± 101.15	2.11	0.09
CHP-212	2.25 ± 0.24	1		N/D			0.37 ± 0.05	1		7.97 ± 0.69	1	
CHP-212Cis100	2.50 ± 0.37	1		N/D			0.70 ± 0.17	1.89		9.55 ± 0.88	1.2	

Values are means ± SD. N/D, not determined due to high intrinsic drug resistance.

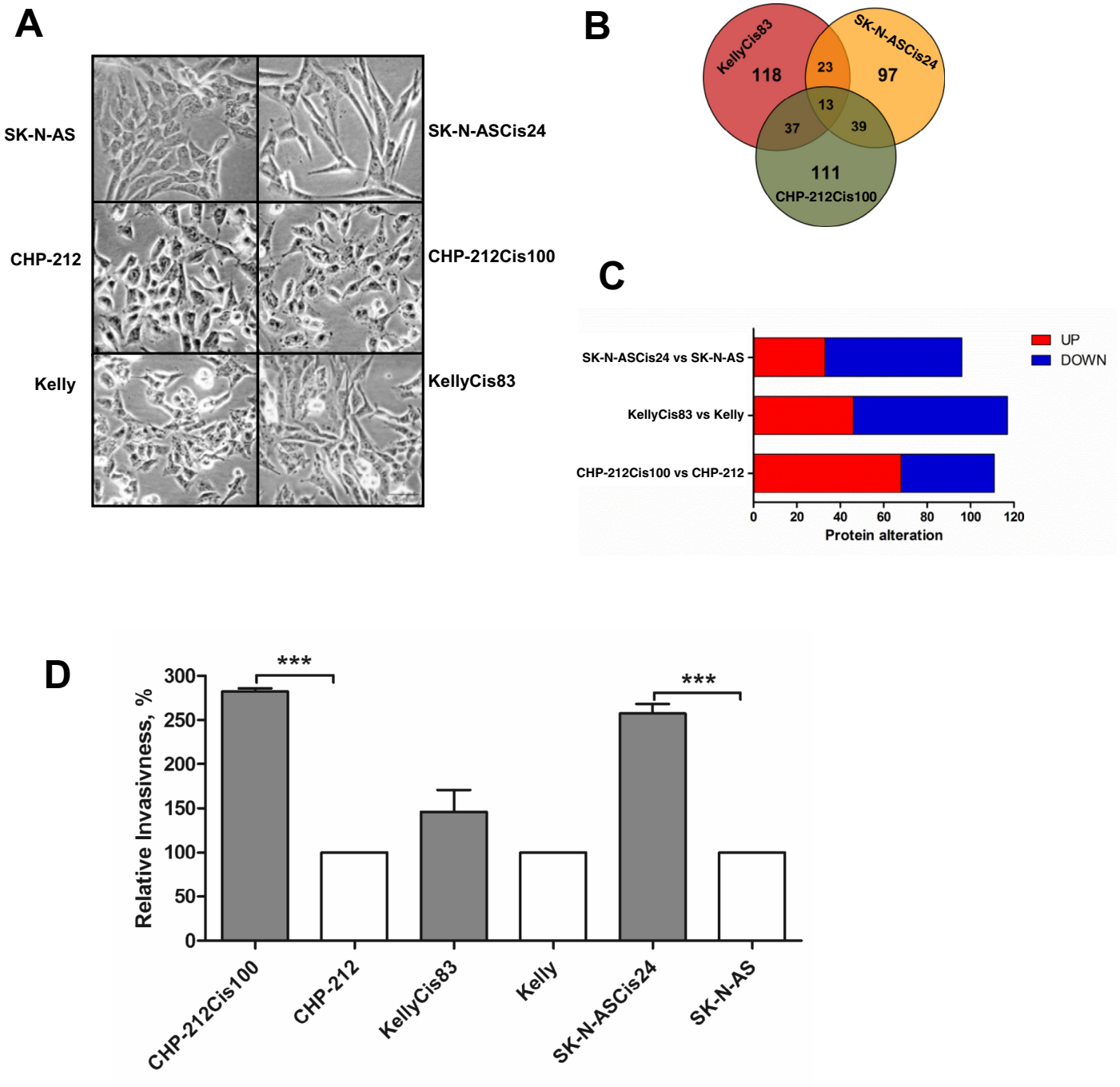

Fig. 1. (A) Morphology changes in cisplatin resistant and corresponding parental cell sub-line. Light phase contrast microscopy, bar 50 µm. (B) Quantitative Venn diagram of the number of identified proteins in three cisplatin resistant cell lines specifying the number of common and exclusively expressed proteins. (C) Summary of down and upregulated proteins across three cisplatin resistant cell lines. (D) Assessment of *in vitro* invasion of CHP-212Cis100 and CHP-212, KellyCis83 and Kelly, SK-N-ASCis24 and SK-N-AS. Graphed data represent mean values ± SD of three independent experiments. Asterisks indicate statistical significance obtained using a paired Student's t-test. * $p < 0.05$, ** $p < 0.01$, *** $p < 0.001$, $n = 3$ for all experiments.

acquisition of a chemotherapeutic drug resistant phenotype. IPA analysis for canonical pathway analysis identified the top 5 pathways for each cisplatin resistant cell line pair (Fig. 2B). Of these, four pathways were common for SK-N-ASCis24 and CHP-212Cis100, while KellyCis83 did not share as many similarities. Only the pathway 'Aldosterone Signaling in Epithelial Cells' was common for KellyCis83 and CHP-212Cis100. IPA analysis for gene networks identified genes involved in DNA replication, recombination and repair, RNA post transcriptional modification, cellular movement and organisation, and inflammatory response (Table 4). All of the above support the concept that drug resistant cells can overcome cytotoxic pressure and adapt through establishment of complicated defence mechanisms which would be unique for each drug resistant tumour [7].

Cisplatin regulator analysis

To explore the possible molecular mechanisms underlying cisplatin resistance, upstream regulator analysis was carried out on the complete datasets of modulated proteins using IPA software. The upstream regulator analysis predicts upstream molecules,

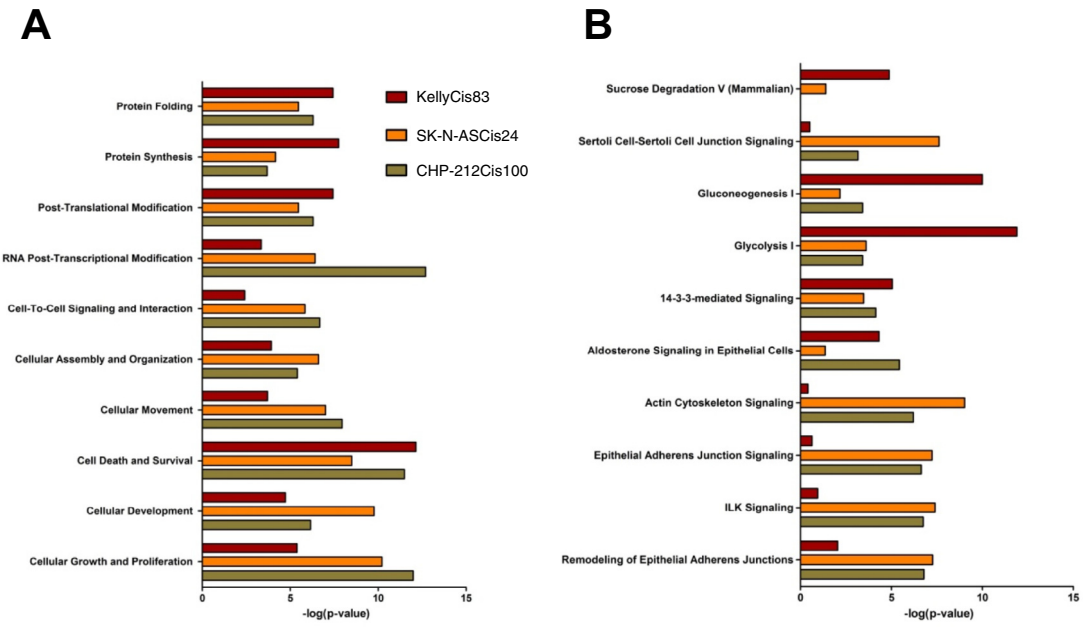

Fig. 2. IPA classification of proteomic data. (A) Classification summary of molecular and cellular functions predicted by IPA. The top 5 functions for each cisplatin resistant cell line were compared. (B) Classification summary of canonical pathways predicted by IPA. The top pathways for each cisplatin resistant cell line were compared. The total bar length is proportional to p value and presented as –log(p value). Coloured blocks next to each function are coded according to cisplatin resistant cell line. Brown – KellyCis83, orange – SK-N-ASCis24 and khaki – CHP-212Cis100.

including microRNA and transcription factors, which may be causing the observed gene expression changes. Known mutual interactions among differentially expressed proteins for each cell line pair were used to construct protein networks ranked by score (Fig. 3). Nine proteins in the cisplatin regulator network were predicted in CHP-212Cis100, 11 in KellyCis83 and 12 in SK-N-ASCis24. Cisplatin regulator network activation z-scores were not significant, –1.029 for CHP-212Cis100, –0.093 for KellyCis83, and 0.637 for SK-N-ASCis24. Four proteins were in common across these networks, beta-tubulin (TUBB), beta-actin (ACTB), vimentin (VIM) and 78 kDa glucose-regulated protein (HSPA5). TUBB had altered expression in the same direction in all drug resistant cells. The rest did not display the same pattern. Increases in VIM expression in SK-N-ASCis24 and CHP-212Cis100 pointed towards a possible epithelial to mesenchymal transition during the development of cisplatin resistance.

Epithelial to mesenchymal transition

A large number of cytoskeletal proteins were identified as having an altered abundance in cisplatin-resistant neuroblastoma cells. Significant modifications in the abundance of cytoskeletal proteins that are consistent with changes associated with epithelial-to-mesenchymal transition (EMT) [8–10] were registered in SK-N-ASCis24 and CHP-212Cis100. These include decreases in cytokeratin proteins (KRT18 and KRT8) and increases in vimentin (VIM) (Table 2). In the case of KellyCis83, a decrease in VIM and no changes in KRT18 and KRT8 were found. The changes in cytoskeletal EMT markers prompted us to examine the expression of known EMT transcription factors SNAI1, ZEB1 and TWIST1 across all three cell line pairs (Fig. 4). Interestingly, the pattern of expression for these three transcription factors was different in parental sensitive cell lines. Kelly and SK-N-AS had higher expression levels of TWIST1 and SNAI1 than ZEB1, while CHP-212–ZEB1 than SNAI1. Loss in the expression of ZEB1 was detected across all resistant cell lines. The resistant CHP-212Cis100 displayed a significant increase of SNAI1 and a decrease of TWIST1 compared to the parental cell line. No change in the levels of SNAI1 and TWIST1 was demonstrated in KellyCis83 and Kelly. The resistant SK-N-ASCis24 displayed significantly lower levels of SNAI1 and TWIST1.

Mesenchymal phenotype of SK-N-ASCis24

As previously mentioned, SK-N-ASCis24 had dramatic changes in its cellular morphology (Fig. 1A), significant modifications in the abundance of cytoskeletal EMT markers, as well as significant modifications in the expression of proteins involved with pathways such as actin cytoskeletal signaling ($p = 9.28E{-}10$), integrin linked kinase (ILK) signaling ($p = 4.01E{-}8$), epithelial adherens junctions signalling ($p = 5.49E{-}{-}8$) and remodelling of epithelial adherens junctions ($p = 5.87E{-}8$) (Fig. 2). All these pathways involve proteins belonging to integrin, actin and myosin families (Fig. 5A). The differential expression for a number of proteins from Fig. 3A has been validated by western blot analysis (Fig. 5B). Proteins of the actin–myosin axes play important roles in mesenchymal cell migration [11], and it is of interest that the SK-N-ASCis24 exhibits a very significant increase in migration potential relative to the parental line (Fig. 1D). All of the above suggests that the cisplatin resistant neuroblastoma cell line SK-N-ASCis24 has acquired a mesenchymal phenotype.

One of the most significant IPA networks that impacted in SK-N-ASCis24 was 'Cellular movement, nervous system development and function, cellular function and maintenance' (Table 4). MYH9, which is known to play an important role in cell motility and invasiveness [12,13], was significantly up-regulated in SK-N-ASCis24 based on mass spectrometry (Table 2) and western blot (Fig. 5B). Over-expression of MYH9 was also detected by immunohistochemical staining of cells (Fig. 5). ROCK/ROK/Rho kinases are also members of the same IPA network as MYH9 (Table 4), and a physical interaction between ROCK1 and MYH9 has been demonstrated [14]. There was no indication by mass spectrometry analysis that ROCK1 expression was modulated in SK-N-ASCis24, although western blot analysis (Fig. 5D–E) and immunohistochemical staining of cells

Table 2
Significantly differentially modulated proteins in cisplatin resistant cell lines in comparison with parental identified by label-free LC-MS.

Accession	Symbol	ID	CHP-212Cis100 versus CHP-212			KellyCis83 versus Kelly			SK-N-ASCis24 versus SK-N-AS		
			Fold change	Modulation	p value	Fold change	Modulation	p value	Fold change	Modulation	p value
P24752	ACAT1	Acetyl-CoA acetyltransferase	1.53	↑	*0.0393088*	0.69	↓	*0.0249396*			
P60709	ACTB	Actin, cytoplasmic 1	0.75	↓	*0.0027265*	0.49	↓	*0.0271745*	1.39	↑	*0.0016375*
P12814	ACTN1	Alpha-actinin-1	0.37	↓	*0.0019869*				3.1	↑	*0.0036693*
O43707	ACTN4	Alpha-actinin-4	0.68	↓	*1.315E-05*				2.02	↑	*0.0104785*
Q09666	AHNAK	Neuroblast differentiation-associated protein AHNAK	1.48	↑	*0.0054692*				0.22	↓	*2.134E-05*
P25705	ATP5A1	ATP synthase subunit alpha	2.15	↑	*0.0019666*	1.49	↑	*0.0176348*			
P06576	ATP5B	ATP synthase subunit beta	1.66	↑	*0.0097048*	1.35	↑	*0.0310778*			
P80723	BASP1	Brain acid soluble protein 1				0.68	↓	*0.0008676*	3.6	↑	*0.0057143*
Q5T1J5	CHCHD2P9	Putative coiled-coil-helix-coiled-coil-helix domain-containing protein CHCHD2P9	1.65	↑	*0.0142642*	1.35	↑	*0.0199838*	0.28	↓	*0.0043879*
Q96EP5	DAZAP1	DAZ-associated protein 1	1.93	↑	*0.0031706*				0.63	↓	*0.0467999*
P60842	EIF4A1	Eukaryotic initiation factor 4A-I	1.55	↑	*0.0001166*				0.43	↓	*0.04885*
P06733	ENO1	Alpha-enolase	0.61	↓	*0.0460728*	1.47	↑	*0.0023987*			
P07954	FH	Fumarate hydratase	1.38	↑	*0.0173403*	0.58	↓	*0.0053465*			
Q96AE4	FUBP1	Far upstream element-binding protein 1				1.47	↑	*0.0111813*	0.62	↓	*0.0317052*
Q14697	GANAB	Neutral alpha-glucosidase AB	1.44	↑	*0.0241526*	0.49	↓	*0.0174452*			
P04406	GAPDH	Glyceraldehyde-3-phosphate dehydrogenase	0.72	↓	*0.0231004*	1.46	↑	*0.0006592*	0.51	↓	*0.0046544*
P0C0S8	HIST1H2AG	Histone H2A type 1	1.7	↑	*0.00082*	0.78	↓	*0.0499551*	0.51		*0.0299902*
P62805	HIST1H4A	Histone H4	1.61	↑	*0.0004494*				0.5	↓	*0.027698*
Q8N257	HIST3H2BB	Histone H2B type 3-B	1.94	↑	*0.0083345*	0.62	↓	*0.0070192*			
P09651	HNRNPA1	Heterogeneous nuclear ribonucleoprotein A1	1.52	↑	*0.023185*				0.57	↓	*0.0006651*
P22626	HNRNPA2B1	Heterogeneous nuclear ribonucleoproteins A2/B1	1.6	↑	*0.0005425*				1.37	↑	*0.0145846*
P51991	HNRNPA3	Heterogeneous nuclear ribonucleoprotein A3	2.29	↑	*0.0012889*				0.06	↓	*0.0218785*
Q14103	HNRNPD	Heterogeneous nuclear ribonucleoprotein D0	1.53	↑	*0.0001069*				0.41	↓	*0.0040732*
P31942	HNRNPH3	Heterogeneous nuclear ribonucleoprotein H3	1.51	↑	*0.0022061*	0.69	↓	*0.0227652*			
P61978	HNRNPK	Heterogeneous nuclear ribonucleoprotein K	1.45	↑	*0.0011688*	1.32	↑	*0.0135432*	0.7	↓	*0.0149234*
P52272	HNRNPM	Heterogeneous nuclear ribonucleoprotein M	1.59	↑	*0.0026679*	1.35	↑	*0.0269281*	0.69	↓	*0.0055936*
Q00839	HNRNPU	Heterogeneous nuclear ribonucleoprotein U	1.57	↑	*0.0088573*	0.6	↓	*0.0095268*			
P08238	HSP90AB1	Heat shock protein HSP 90-beta	1.27	↑	*0.0215486*	1.24	↑	*0.0022558*			
P11021	HSPA5	78 kDa glucose-regulated protein	1.38	↑	*0.0014272*	0.62	↓	*0.039906*	3.18	↑	*0.0072475*
P38646	HSPA9	Stress-70 protein	1.59	↑	*1.751E-07*	0.62	↓	*0.007537*			
P04792	HSPB1	Heat shock protein beta-1	0.43	↓	*0.0003869*				0.42	↓	*0.0264504*
P10809	HSPD1	60 kDa heat shock protein	1.75	↑	*0.0001189*	0.78	↓	*0.0075304*			
P61604	HSPE1	10 kDa heat shock protein	2.04	↑	*0.0047056*	0.69	↓	*0.0237272*			
Q92945	KHSRP	Far upstream element-binding protein 2	1.6	↑	*0.0056766*				0.57	↓	*0.0237794*
P52292	KPNA2	Importin subunit alpha-2				3.28	↑	*0.0043833*	1.98	↑	*0.0342929*
P05783	KRT18	Keratin, type I cytoskeletal 18	0.11	↓	*3.135E-05*				0.12	↓	*0.0003971*

(*continued on next page*)

Table 2 (*continued*)

Accession	Symbol	ID	CHP-212Cis100 versus CHP-212			KellyCis83 versus Kelly			SK-N-ASCis24 versus SK-N-AS		
			Fold change	Modulation	p value	Fold change	Modulation	p value	Fold change	Modulation	p value
P05787	KRT8	Keratin, type II cytoskeletal 8	0.07	↓	*3.173E-10*				0.05	↓	*0.0068007*
P00338	LDHA	L-lactate dehydrogenase A chain				1.23	↑	*0.0137737*	0.5	↓	*0.0297607*
P07195	LDHB	L-lactate dehydrogenase B chain				0.56	↓	*0.0009125*	0.29	↓	*0.0084766*
P46821	MAP1B	Microtubule-associated protein 1B	1.34	↑	*0.0065255*	1.63	↑	*0.0078873*			
P40926	MDH2	Malate dehydrogenase	1.67	↑	*0.0188808*	1.54	↑	*0.0069937*			
P35579	MYH9	Myosin-9	0.6	↓	*0.027779*				4.27	↑	*0.0040361*
O14950	MYL12B	Myosin regulatory light chain 12B	0.5	↓	*0.0259878*				3.03	↑	*0.0132585*
P60660	MYL6	Myosin light polypeptide 6	0.69	↓	*0.0110096*				2.54	↑	*0.0028463*
Q15843	NEDD8	NEDD8				0.52	↓	*0.0355481*	0.32	↓	*0.0270897*
Q15233	NONO	Non-POU domain-containing octamer-binding protein	1.6	↑	*4.498E-05*				0.7	↓	*0.014344*
P06748	NPM1	Nucleophosmin	1.34	↑	*0.0060107*				1.31	↑	*0.0025631*
P07237	P4HB	Protein disulfide-isomerase	0.48	↓	*0.0259334*				3.17	↑	*0.0067148*
P30101	PDIA3	Protein disulfide-isomerase A3	0.58	↓	*0.0001215*	0.71	↓	*0.041118*	2.94	↑	*0.0120008*
Q15084	PDIA6	Protein disulfide-isomerase A6				0.62	↓	*0.0460694*	2.16	↑	*0.0171422*
P07737	PFN1	Profilin-1	0.62	↓	*0.0087943*	1.58	↑	*0.0021374*	0.35	↓	*0.0169905*
P00558	PGK1	Phosphoglycerate kinase 1				1.48	↑	*0.0295475*	0.47	↓	*0.0380779*
P35232	PHB	Prohibitin	1.75	↑	*0.0087227*	0.71	↓	*0.0037858*	0.32	↓	*0.0075181*
P14618	PKM	Pyruvate kinase isozymes M1/M2	0.66	↓	*0.0018889*	1.49	↑	*0.0111613*			
Q06830	PRDX1	Peroxiredoxin-1	1.49	↑	*0.0066261*	0.03	↓	*0.0315948*	0.64	↓	*0.0301092*
P30041	PRDX6	Peroxiredoxin-6	0.71	↓	*0.0390701*				0.53	↓	*0.0101555*
P62979	RPS27A	Ubiquitin-40S ribosomal protein S27a	0.51	↓	*0.0334092*	1.56	↑	*0.0180621*			
P08865	RPSA	40S ribosomal protein	1.58	↑	*0.0140854*	0.67	↓	*0.00124*			
P82979	SARNP	SAP domain-containing ribonucleoprotein	0.73	↓	*0.0372508*				0.67	↓	*0.0050523*
P23246	SFPQ	Splicing factor, proline- and glutamine-rich	1.82	↑	*0.0106231*	1.46	↑	*0.0395062*			
Q01082	SPTBN1	Spectrin beta chain, non-erythrocytic 1	0.54	↓	*0.0004211*				1.68	↑	*0.0007724*
Q9UJZ1	STOML2	Stomatin-like protein 2	4.31	↑	*0.0004175*	0.65	↓	*0.0141966*			
P29401	TKT	Transketolase	0.29	↓	*9.695E-05*	0.58	↓	*0.0001948*			
P60174	TPI1	Triosephosphate isomerase				1.58	↑	*0.0020865*	0.48	↓	*0.0301769*
Q9BQE3	TUBA1C	Tubulin alpha-1C chain	0.77	↓	*0.0031913*				0.6	↓	*0.0164661*
P07437	TUBB	Tubulin beta chain	0.78	↓	*0.0455105*	0.35	↓	*0.000303*	0.37	↓	*0.0423107*
Q15819	UBE2V2	Ubiquitin-conjugating enzyme E2 variant 2				0.59	↓	*0.0090759*	0.32	↓	*0.0474067*
P18206	VCL	Vinculin	0.53	↓	*0.0088382*				0.56	↓	*0.0260816*
P55072	VCP	Transitional endoplasmic reticulum ATPase	1.9	↑	*0.0067195*	0.58	↓	*0.0048664*			
P08670	VIM	Vimentin	1.33	↑	*0.0224295*	0.07	↓	*0.0007459*	4.83	↑	*0.0040634*
P13010	XRCC5	X-ray repair cross-complementing protein 5	4.78	↑	*0.0012141*	0.7	↓	*0.0204185*			
P61981	YWHAG	14-3-3 protein gamma	0.68	↓	*6.034E-05*				0.74	↓	*0.0433372*
P63104	YWHAZ	14-3-3 protein zeta/delta	0.7	↓	*0.0406417*	0.7	↓	*0.0282821*			

Table 3
List of proteins identified in top scoring molecular and cellular functions predicted by IPA.

Function	Name	p-value	Molecules
Cellular growth and proliferation	CHP-212Cis100	5.54E–10	HNRNPL, SRSF2, DBN1, NPM1, PFN1, S100A11, GNB2L1, SFPQ, HSPA5, TUBB, LMNB1, CACYBP, HNRNPA1, TARDBP, HNRNPF, YWHAG, CFL1, ATP5A1, RPL23A, SRSF3, CBX1, ATP5B, LMNB2, ZYX, ACTN4, VDAC1, XRCC5, HNRNPAB, RPSA, SPTBN1, PRDX1, PDIA3, HNRNPA2B1, PKM, HNRNPK, UCHL1, PHB, HSP90AB1, AHNAK, FLNA, ANXA1, VCP, VCL, NCL, HNRNPC, ACTN1, HNRNPU, ACTB, G6PD, VIM, HNRNPD, HSPD1, ACLY, HNRNPM, ENO1, KRT8, DAZAP1, SERPINH1, EIF4A1, ACAT1, MYH9
	KellyCis83	2.97E–04	CHGA, PFN1, EML4, CCT2, RAN, UBE2V2, SFPQ, TUBB, HSPA5, EIF3C/EIF3CL, STMN1, ENAH, PGK1, CDC37, EWSR1, ATP5A1, CLTC, PFDN5, HSPA8, PTBP1, ATP5B, FSCN1, XRCC5, GSTP1, RPSA, PRDX2, PEBP1, NME1, PRDX1, PDIA3, KPNA2, PKM, EEF1B2, DDX17, IGF2BP1, HNRNPK, HSP90AB1, PHB, VCP, PFN2, HNRNPU, TRIM28, VIM, HSPD1, HNRNPM, ENO1, GPI, ACAT1, CCT7, GAP43
	SK-N-ASCis24	5.04E–08	NPM1, TPD52L2, PFN1, SEPT9, NME2, UBE2V2, HSPA5, TUBB, CTSD, HNRNPA1, FASN, S100A10, PGK1, YWHAG, PLEC, LMNA, NASP, LIMA1, SPTAN1, ACTN4, CTTN, LDHA, SPTBN1, PRDX1, PDIA3, KPNA2, HNRNPA2B1, NAA10, HNRNPK, PHB, AHNAK, HNRNPR, VCL, ACTN1, ITGB1, CALR, PTMA, ACTB, ITGA2, VIM, HNRNPD, NAP1L1, HNRNPM, COL1A1, ALB, KRT8, DAZAP1, NT5E, EIF4A1, CRABP2, CD44,MYH9
Cell death and survival	CHP-212Cis100	9.59E–10	SRSF2, NPM1, S100A11, MAP1B, GNB2L1, SFPQ, HSPA5, TUBB, LMNB1, CACYBP, HNRNPA1, TARDBP, P4HB, YWHAG, CFL1, ATP5A1, HSPA9, YWHAZ, STOML2, HSP90AA1, ZYX, KRT18, ACTN4, AARS, FH, VDAC1, XRCC5, RPSA, HSPB1, HSD17B10, SPTBN1, FLNB, PDIA3, PRDX1, PKM, GAPDH, HNRNPK, PRDX6, ATP5H, UCHL1, PHB, HSP90AB1, FLNA, ANXA1, ANXA5, HSPE1, VCP, VCL, NCL, HNRNPC, HNRNPU, ACTB, G6PD, VIM, HSPD1, ACLY, ENO1, KRT8, ACAT1, MYH9
	KellyCis83	2.44E–10	CHGA, EEF1A2, MAP1B, CCT2, RAN, UBE2V2, SFPQ, HSPA5, CBX5, TUBB, EIF3C/EIF3CL, VDAC2, STMN1, RUVBL2, ALDOC, CDC37, EWSR1, YWHAE, EEF2, BLVRA, YWHAB, ATP5A1, HSPA9, BASP1, YWHAZ, PHB2, STOML2, FUBP1, RANBP1, HSPA8, STIP1, ALDOA, FH, GSTP1, XRCC5, RPSA, PRDX2, PEBP1, NME1, PRDX1, PDIA3, KPNA2, PKM, GAPDH, DDX17, EIF2S1, IGF2BP1, HNRNPK, CCT4, ALDH2, HSP90AB1, PHB, VCP, HSPE1, NEDD8, HNRNPU, TRIM28, VIM, HSPD1, ENO1, GPI, ACAT1, CCT7, MAOA, PAFAH1B3
	SK-N-ASCis24	1.29E–06	SPTBN1, NPM1, PRDX1, PDIA3, HLA-A, KPNA2, GAPDH, NME2, UBE2V2, KIAA1967, HSPA5, TUBB, HNRNPK, PRDX6, CTSD, HNRNPA1, PHB, FASN, NEDD8, VCL, RPS3, ACTC1, S100A10, ITGB1, CALR, P4HB, PTMA, YWHAG, ACTB, ITGA2, BASP1, PLEC, VIM, LMNA, FUBP1, COL1A1, ALB, KRT8, NT5E, CRABP2, CD44, MYH9, KRT18, ACTN4, CNPY2, CTTN, LDHA, HSPB1
Cellular movement	CHP-212Cis100	2.13E–06	HNRNPL, DBN1, NPM1, FLNB, PFN1, PRDX1, HNRNPA2B1, GNB2L1, MAP1B, PKM, HSPA5, LMNB1, HNRNPK, HSP90AB1, PHB, FLNA, ANXA5, ANXA1, TUBA1C, VCL, NCL, CFL1, ACTB, G6PD, YWHAZ, VIM, HSPD1, KRT8, MYL12B, ACAT1, HSP90AA1, ZYX, MYH9, LMNB2, ACTN4, FH, RPSA, HSPB1
	KellyCis83	6.21E–03	PEBP1, DPYSL2, NME1, CHGA, PFN1, PRDX1, KPNA2, EEF1A2, PKM, MAP1B, CBX5, HSPA5, IGF2BP1, HNRNPK, TUBB2B, STMN1, ENAH, HSP90AB1, PHB, YWHAE, YWHAZ, VIM, HSPD1, GPI, FLNC, FSCN1, ACAT1, ALDOA, GAP43, FH, RPSA, MAOA
	SK-N-ASCi24	1.91E–05	NPM1, PFN1, SEPT9, PRDX1, KPNA2, HNRNPA2B1, NME2, HSPA5, HNRNPK, CTSD, PHB, FASN, TUBA1C, VCL, S100A10, ITGB1, CALR, PTMA, ACTB, ITGA2, PLEC, VIM, LMNA, COL1A1, ALB, KRT8, MYL12B, NT5E, LIMA1, CD44, MYH9, ACTN4, CTTN, HSPB1
Cell-to-cell signaling and interaction	CHP-212Cis100	2.66E–05	FLNB, SRSF2, DBN1, NPM1, PFN1, CFL1, ACTB, GNB2L1, VIM, UCHL1, KRT8, FLNA, ANXA1, ANXA5, ZYX, MYH9, KRT18, VCL, ACTN4, ACTN1, RPSA
	KellyCis83	3.53E–02	DPYSL2, GPI, NME1, CHGA, PDIA3, KPNA2, VIM, GAP43, MAOA
	SK-N-ASCis24	1.38E–04	NPM1, PFN1, PDIA3, HLA-A, KPNA2, HSPA5, CTSD, VCL, ACTN1, S100A10, ITGB1, CALR, ACTB, ITGA2, PLEC, VIM, COL1A1, KRT8, NT5E, LIMA1, CD44, MYH9, KRT18, ACTN4, SPTAN1, CTTN
Cellular development	CHP-212Cis100	5.63E–05	HNRNPL, SPTBN1, FLNB, DBN1, NPM1, SRSF2, PFN1, PDIA3, MAP1B, PKM, GNB2L1, HNRNPA2B1, GAPDH, SFPQ, HSPA5, TUBB, LMNB1, HNRNPK, UCHL1, CACYBP, HNRNPA1, HSP90AB1, PHB, FLNA, ANXA1, CALD1, TARDBP, PHGDH, NCL, YWHAG, CFL1, ACTB, YWHAZ, G6PD, VIM, HSPD1, ACLY, SRSF3, ENO1, CBX1, KRT8, EIF4A1, ACAT1, LMNB2, HSP90AA1, ACTN4, XRCC5
	KellyCis83	9.89E–04	DPYSL2, PEBP1, CHGA, NME1, PFN1, PDIA3, KPNA2, MAP1B, CCT2, PKM, RAN, EEF1B2, SFPQ, DDX17, HSPA5, TUBB, EIF3C/EIF3CL, HNRNPK, IGF2BP1, IDH1, STMN1, PHB, VCP, PFN2, CDC37, EWSR1, TRIM28, BASP1, PFDN5, PTBP1, GPI, FSCN1, STIP1, ACAT1, GAP43, XRCC5, SEPT2, PRDX2
	SK-N-ASCis24	1.04E–07	NPM1, PFN1, SEPT9, PDIA3, KPNA2, HNRNPA2B1, NME2, NAA10, TUBB, HSPA5, HNRNPK, CTSD, HNRNPA1, PHB FASN, VCL, S100A10, ITGB1, PGK1, CALR, PTMA, YWHAG, ACTB, ITGA2, COL1A1, NASP, KRT8, EIF4A1, CRABP2, CD44, ACTN4, SPTAN1, CTTN, LDHA

(Fig. 5F) indicated a lower level of expression of ROCK1, which might be consistent with the mesenchymal phenotype, as will be discussed later.

Discussion

Whether pre-existent (intrinsic), or induced by treatment (acquired), drug resistance involves complex changes at both genetic and epigenetic levels. These can vary across different cancers and present the major impediment to the successful treatment of disease. Understanding the pathophysiology underlying intrinsic or acquired resistance will be paramount to stratifying patients into subgroups and subsequent design of new therapies and treatment regimens. This is particularly important for neuroblastoma, which is a highly heterogeneous disease where recurrence and progression is very common in spite of intensive multimodal therapy [1].

Several groups have developed drug resistant neuroblastoma cell lines in order to elucidate the mechanisms and key players involved in this process. To date, 14 clinically relevant drug resistant neuroblastoma cell lines have been published [5,15–22]. Unfortunately, it is difficult to make a direct comparison between them as they have very little overlapping characterisation.

In the present study, we characterised three cisplatin resistant neuroblastoma cell lines to gain insights in similarities and differences between them. The morphological and growth characteristics were documented for the three resistant cell lines. Of these, SK-N-ASCis24 underwent the most dramatic morphological changes during the development of drug resistance, and the most significant changes in cell invasiveness. Similarly, significant morphology changes were observed for UKF-NB-2 resistant derivatives [16,18]. The fact that the doubling time of SK-N-ASCis24 was significantly higher indicates that the invasive potential of the cells was altered, as opposed to an increase in the number of cells available to cross the

Table 4
Top scoring network predicted by IPA. Proteins identified in our datasets are capitalised in bold.

Cell line	Associated network	Score	Focus molecules	Molecules in network
CHP-212Cis100	RNA post-transcriptional modification, connective tissue disorders, metabolic disease	77	32	**AHNAK**, Akt, **HIST2H2BF, HN1, HNRNPA1, HNRNPA2B1, HNRNPAB, HNRNPC, HNRNPD, HNRNPF, HNRNPH1, HNRNPH3, HNRNPK, HNRNPL, HNRNPM, HNRNPU, HSPA9, KCTD12, KHSRP, MAP1B, NCL, NONO, NPM1**, p85 (pik3r), **RBM14**, Rnr, **RPL23A, S100A16, SFPQ, SRSF2, SRSF3, TARDBP, TKT, XRCC5, YWHAZ**
	Immunological disease, dermatological diseases and conditions, inflammatory disease	37	20	**AARS, ACTB,** Actin, **ACTN1, ACTN4,** Alpha Actinin, Alpha catenin, **ANXA1, ANXA5, CACYBP, CALD1, CFL1**, Cofilin, **DBN1, ENO1, ERK1/2,** F Actin, G-Actin, Lamin b, Mlc, **MYH9, MYL6, MYL12B**, Myosin, **PDGF** (family), **PFN1,** Profilin, Rock, **S100A11**, **SPTBN1, TPM4,** Tropomyosin, trypsin, **VCL, ZYX**
	Nucleic acid metabolism, small molecule biochemistry, DNA replication, recombination, and repair	35	18	14-3-3, adenosine-tetraphosphatase, ATP synthase, **ATP5A1, ATP5B, ATP5H,** ATPase, caspase, cytochrome C, cytochrome-c oxidase, **FH, G6PD, HSD17B10,** Hsp27, Hsp70, Hsp90, **HSP, HSP90AA1, HSPA5, HSPB1, HSPD1, HSPE1, KRT8, LMNB1, LMNB2, MAP2K1/2, MDH2,** NFkB (complex), Pkg, **PRDX1**, Raf, Rsk, Ubiquitin, **VCP, VIM**
	Cellular movement, cellular assembly and organisation, cellular function and maintenance	32	17	Alpha tubulin, Beta Tubulin, calpain, CaMKII, Cdc2, Collagen type I, Collagen(s), Cytokeratin, **ERK, FLNA, FLNB**, Focal adhesion kinase, **GANAB, GAPDH, GNB2L1, HISTONE, HSP90AB1**, Integrin, **KRT18,** Laminin, **P4HB, PDGF BB, PHB, PSAT1, RPSA, SERPINH1,** Sos, **STOML2, TCR,** Tgf beta, **TUBA1C, TUBB**, Tubulin, **VDAC1, YWHAG**
	Molecular transport, RNA trafficking, protein synthesis	18	11	60S ribosomal subunit, **ANKRD13B, BRD7**, C15orf39**, CHD1L, DAZ1/DAZ4, DAZAP1, DAZL, DPP7, EIF4A1, EIF4H, H3F3C, HIST3H2A, HIST3H2BB, HNRNPA3, MPC2, MRPL12, MT-ND2, MYLK3, MYLK, PKP1, RBMXL1, RCHY1, RPL14, RPL17, RPL21, RPL34, RPL39, RPL26L1, RPLP1, SARNP, SYPL1, THOC6, TSPY8, UBC**
KellyCis83	RNA post-transcriptional modification, molecular transport, protein trafficking	60	27	**CBX5, DDX1, DDX17,** E2f, **EIF3C/EIF3CL, FUBP1, GANAB, GAP43, HIST2H2AB, HIST3H2BB,** Histone H1, Histone h4, **HNRNPH3, HNRNPK, HNRNPM, HNRNPU, IGF2BP1, KPNA2, MATR3, NEDD8**, NFkB (complex), **NHP2L1, PEBP1, PTBP1, RAN**, Ribosomal 40s subunit, RNA polymerase II, Rnr, **RPS7, RPS27A, RPSA, RUVBL2, SFPQ**, thymidine kinase, **XRCC5**
	Cellular assembly and organisation, cellular function and maintenance, tissue development	47	23	14-3-3, Actin, Akt, Alpha tubulin, Beta Tubulin, **BLVRA, CCT2, CCT4, CCT7, CHGA, CLTC, DPYSL2, EEF2, EIF4A, EIF4H, ENAH,** F Actin, **FSCN1, GPI**, Importin alpha, **MAP1B, PDIA6, PFDN2, PFDN5, PFN1, PFN2, PP2A**, Profilin, Rock, **SEPT2, STMN1, TUBB, TUBB2B**, Tubulin, **YWHAZ**
	Haematological disease, immunological disease, inflammatory disease	46	22	14-3-3 (β,ε,ζ), adenosine-tetraphosphatase, **ALDH2,** aldo, ATP synthase, **ATP5A1, ATP5B, ATP5J, ATP6V1A**, ATPase, **CDC37**, creatine kinase, cytochrome-c oxidase, **EEF1B2, ERK1/2, FH, GAPDH**, hemoglobin, Hsp70, **HSP, HSPA9, HSPD1, HSPE1, MDH2, PDGF** (family), **PDIA3, PHB, PRDX1, PRDX2**, Rsk, **STIP1, STOML2, TKT, VDAC2, YWHAE**
	Hereditary disorder, neurological disease, psychological disorders	28	15	**ACAT1, ADRB, ALDOA, ALDOC, BCR** (complex), caspase, Dynamin, **EEF1A2, EIF2S1, ERK, HSPA5, IDH1**, Ikb, Immunoglobulin, Insulin, Ldh, **LDHB, LDL, MAP2K1/2,** Mek, **NME1,** p70 S6k, **PAFAH1B3, PGK1, PITPNB**, Pkc(s), PP1 protein complex group, Proinsulin, **RANBP1, RCN1**, Sos, STAT5a/b, **TCR**, Ubiquitin, YWHAB
	Cancer, gastrointestinal disease, hepatic system disease	22	13	26s Proteasome, **AMPK, BASP1**, Calmodulin, calpain, CaMKII, **CD3, CRABP1**, cytochrome C, **EIF4A2, ENO1**, estrogen receptor, **EWSR1, FLNC, FSH, GSTP1**, Histone h3, Hsp90, **HSP90AB1, HSPA8**, Interferon alpha, Jnk, Lh, Mapk, **P38 MAPK**, p85 (pik3r), **PHB2, PI3K** (complex), Pka, **PKM**, **PLC gamma**, Rb, **VCP**, Vegf, **VIM**
SK-N-ASCis24	Haematological disease, immunological disease, inflammatory disease	56	25	**ACTB, ACTN1**, Akt, **ALB**, Alpha actin, Beta Tubulin, **CFL2, DAZAP1,** F Actin, G-Actin, **GAPDH**, Growth hormone, **HIST1H2BB, HNRNPA3, HNRNPD, KHSRP, KRT8**, Lamin b, Ldh, **LDHA, LDHB, LIMA1, LUC7L2, NASP, NEDD8, PI3K** (family), **PLEC, PRDX1, PRDX6**, Spectrin, **SPTAN1, SPTBN1, TUBA1C, TUBB, YWHAG**
	Developmental disorder, gastrointestinal disease, hepatic system disease	31	16	**ADAMTS4, ANXA11, B4GALT1, BROX, CHMP4B, CNPY2, CNPY3, CTH, CYB5R1, DPP8, EIF4A1, IDO1, IL10RA, ITPRIPL1, JAG1, KIAA1967, KLF6, MXRA7, NOTCH2, NPR1, NT5E, PTMA, RPLP2, SARNP, SCAF1, SEPT9, SP7, SRP9, TNF**, TPI1, **TSC22D3, UBC, UBE2V2, UBQLN4, VAT1**
	Cell morphology, cellular function and maintenance, DNA replication, recombination, and repair	31	16	14-3-3, 26s Proteasome, Actin, Alpha tubulin, BCR (complex), caspase, Cdc2, Cytokeratin, E2f, **FUBP1, HISTONE, HLA-A**, Hsp27, Hsp70, Hsp90, **HSPA5, HSPB1,** Ifn, **KPNA2, KRT18, MHC Class I** (complex), **NAA10, NAP1L1**, NFkB (complex), **NPM1, PDIA4 ,PHB,** Pmca, **PSME1, PTMA**, Rnr, **RPS3, S100A10**, Ubiquitin, **VIM**
	Amino acid metabolism, post-translational modification, small molecule biochemistry	26	14	**ACTN4**, Alpha Actinin, Alpha catenin, C1q, calpain, **CALR, COL1A1**, Collagen Alpha1, Collagen type I, Collagen type III, Collagen type IV, Collagen(s), **CTTN, ERK1/2**, Fibrinogen, Integrin, Integrin alpha 2 beta 1, Integrin alpha 5 beta 1, **ITGA2, ITGB1**, **JINK1/2,** Laminin, **LAP3**, Lfa-1, **NME2, P4HA1, P4HB, PDGF** (family), **PDIA3, PDIA6,** Talin, Tap, **TPD52L2, VCL**, Vla-4
	Cellular movement, nervous system development and function, cellular function and maintenance	22	13	**ACTC1, AHNAK**, Ap1, ATPase, **BASP1**, Calmodulin, CaMKII, **CD3, CD44**, Ck2, Cofilin, **CRABP2**, Creb, **ERK, FASN**, Focal adhesion kinase, **HNRNPA1, HNRNPR, MAP2K1/2**, Mlc, **MYH9, MYL6, MYL12B, P38 MAPK**, p70 S6k, **PDGF BB, PFN1, PGK1, PLC** gamma, **PP2A**, Ras, Rock, Sos, **TCR**, Tgf beta

membrane. Consistent with this observation is the fact that the proteomics profile showed an increase in several proteins that play key roles in cytoskeletal structure and cell invasion. This includes proteins of integrin (ITGB1, ITGA2), actin (ACTB, ACTN1, ACTN4, ACTC1) and myosin (MYH9, MYL12B, MYL6) families.

KellyCis83 and SK-N-ASCis24 display levels of cisplatin resistance comparable with that exhibited by neuroblastoma cell lines derived from tumours at different phases of chemotherapy [23]. These resistance patterns correlated well with both treatment intensities and drugs that the patients were administrated. Therefore, drug resistant cell lines KellyCis83 and SK-N-ASCis24 exhibit clinically relevant cisplatin resistant patterns. It appears that the SK-N-AS cell line is more sensitive to cisplatin than the other tested drugs in our study and as a result required lower doses of cisplatin to acquire drug resistance. This observation is in agreement with Prochazka's study, where low doses of cisplatin were applied for the generation of another drug resistant SK-N-AS subline [15].

Cisplatin is known to induce cross resistance to a variety of drugs. We examined cross resistance of cisplatin resistant neuroblastoma cell lines to combination drugs used in neuroblastoma chemotherapy, namely temozolomide (alkylating agent), etoposide and irinotecan (topoisomerase inhibitors). The IC50 values of the

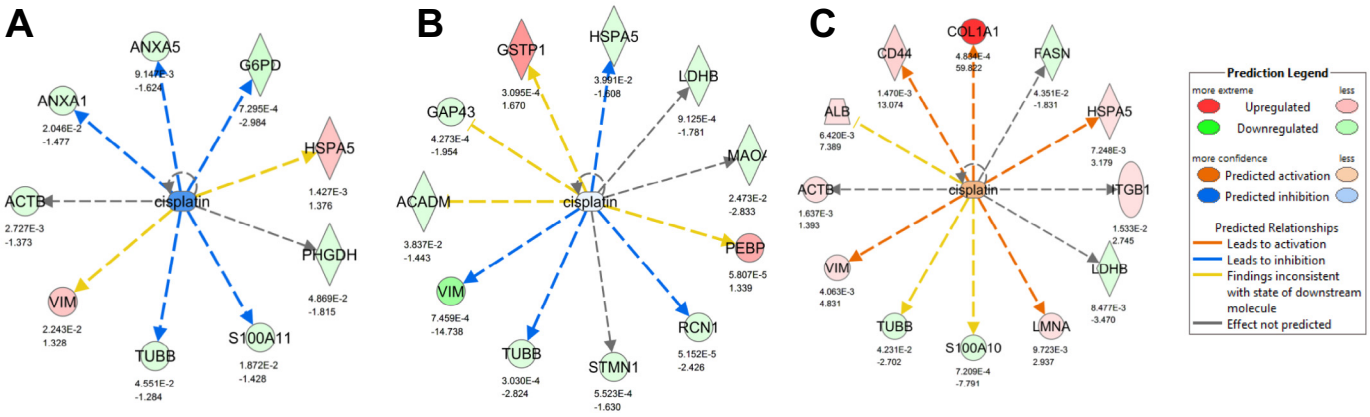

Fig. 3. Cisplatin regulator network analysis. IPA prediction of upstream molecules in cisplatin regulator network activation from the modulated protein datasets. (A) CHP-212Cis100, (B) KellyCis83 and (C) SK-N-ASCis24. Legend key of IPA prediction is in the right corner.

resistant cell sublines were 1.3–2.8-fold higher in response to topoisomerase inhibitors than that of their respective parental cell lines. This is consistent with published data demonstrating that cisplatin can induce cross resistance to multiple drugs both *in vitro* [24,25] and in clinical settings [23,26]. No significant changes were detected for an alkylating drug, temozolomide across all three resistant cell lines. Hence, the observed significant resistance to irinotecan, which is currently used routinely for relapsed high risk neuroblastoma [27], may provide vital information on the potential mechanisms of resistance to the re-initiation therapy.

Despite significant phenotypic changes, increased invasiveness, accumulation of genomic aberrations and altered protein expression, no significant difference in the IC50 of CHP-212Cis100 compared to its parental cell line was detected, which may be due

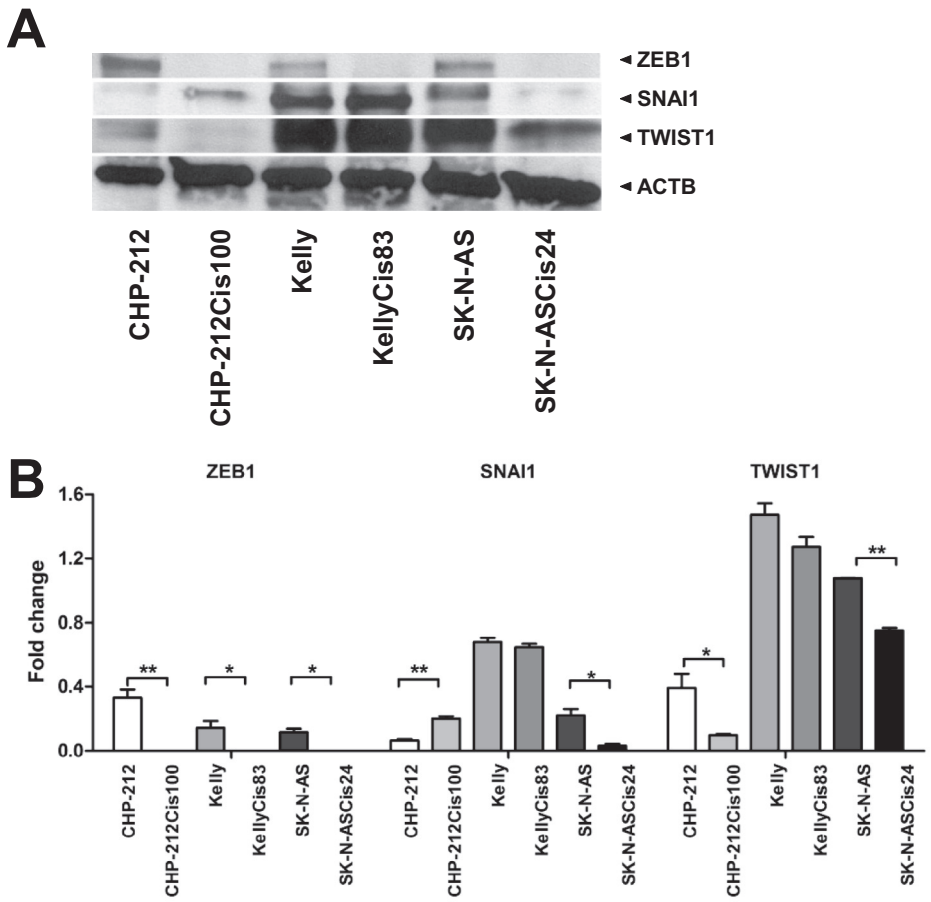

Fig. 4. Epithelial to mesenchymal transition markers. (A) Representative image of western blot analysis of three cisplatin resistant and sensitive cell line pairs using the indicated antibodies. TWIST1, SNAI1 and ZEB1 were probed on the same blot. Typically, 5 μg of protein extract was loaded per well, equal loading was confirmed by Coomassie blue staining (Supplementary File S4). (B) The fold change in protein expression of drug resistant cells compared to their parental counterparts was quantified by densitometric analysis of two biological repeat experiments, normalised against endogenous control ACTB.

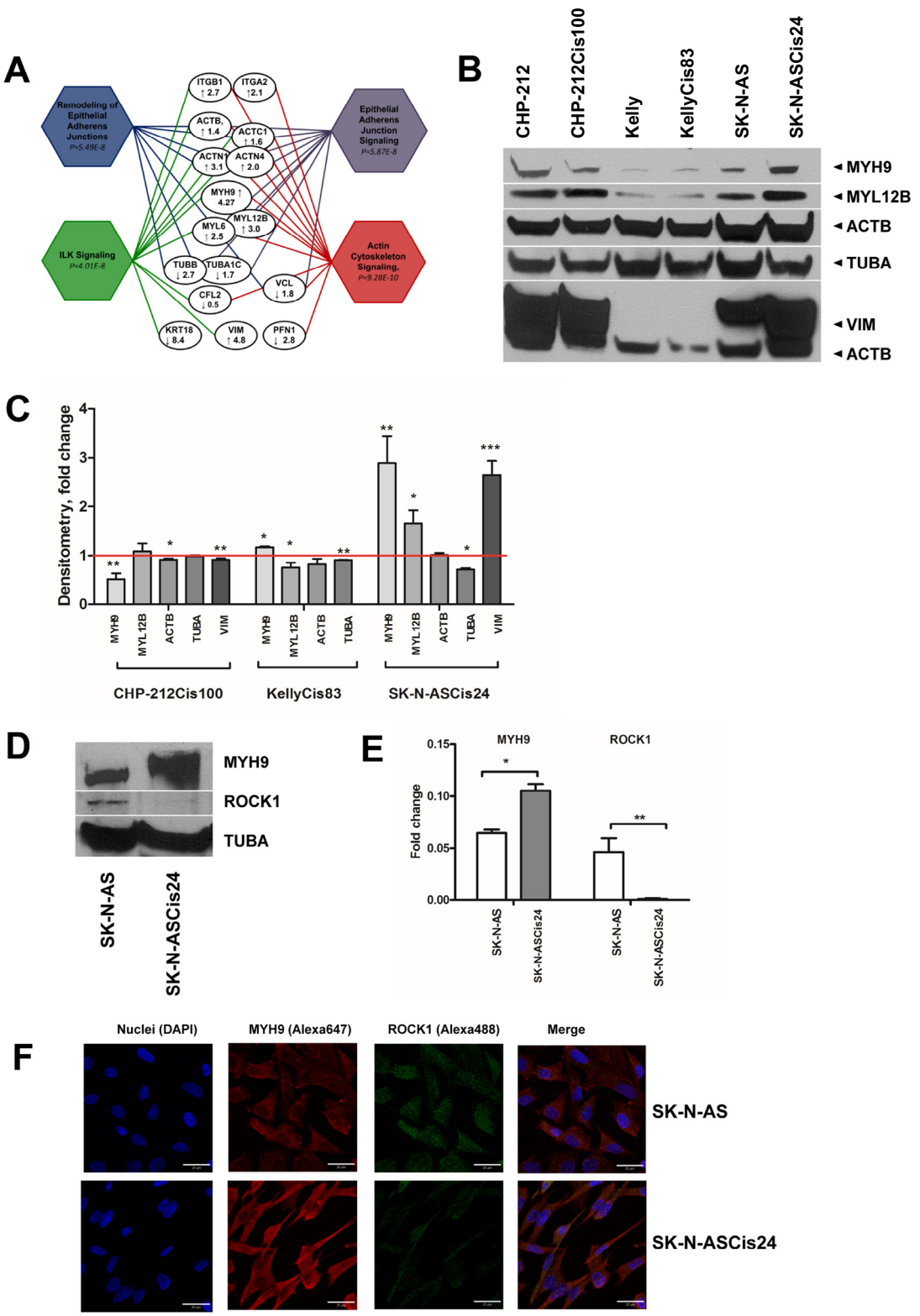

Fig. 5. Mesenchymal phenotype. (A) Common proteins in common IPA pathways. (B) Representative image of western blot analysis of three cisplatin resistant and sensitive cell line pairs using the indicated antibodies. MYH9, MYL12B, ACTB were probed on the same blot, while VIM and ACTB on the other and TUBA separately. Typically, 5 μg of protein extract was loaded per well, equal loading was confirmed by Coomassie blue staining (Supplementary File S4). (C) The fold change in the protein expression of drug resistant cells compared to their parental counterparts was quantified by densitometric analysis of two biological repeat experiments. The red horizontal line represents protein expression in parental cell lines. Graphed data represent mean values ± SD of three independent experiments. Asterisks indicate statistical significance obtained using a paired Student's t-test. * $p < 0.05$, ** $p < 0.01$, *** $p < 0.001$, $n = 3$ for all experiments. (D) Representative image of western blot analysis of SK-N-ASCis24 and SK-N-AS cells with anti-MYH9, anti-ROCK1 and TUBA antibodies. (E) The fold change in protein expression of drug resistant cells compared to their parental counterparts was quantified by densitometric analysis of two biological repeat experiments, normalised against endogenous control TUBA. The red horizontal line represents protein expression in parental cell lines. Graphed data represent mean values ± SD of three independent experiments. Asterisks indicate statistical significance obtained using a paired Student's t-test. * $p < 0.05$, ** $p < 0.01$, *** $p < 0.001$. (F) Immunostaining of SK-N-ASCis24 and SK-N-AS cells with anti-MYH9 and anti-ROCK1 antibodies followed by visualisation with AlexaFluor-647 and Alexa Fluor-488, respectively. Bar, 25 μm.

to the intrinsic resistance of parental CHP-212 to cisplatin, with IC50s equal to or greater than those of both the resistant Kelly and SK-N-AS lines. This high level of intrinsic resistance explains the much higher concentrations of cisplatin required to select a CHP-212 resistant variant. Little information is available about intrinsic resistance in neuroblastoma; however the association between chemoresistance and enhanced pro-angiogenic activity has been observed and deemed relevant for tumor progression [28,29]. It is possible that the CHP-212 cell line represents a sub-population of cells with intrinsic resistance in neuroblastoma, in which case the characterisation of both CHP-212 and CHP-212Cis100 will prove useful for future studies of drug resistance.

Once drug resistance was confirmed, additional functional effects were investigated to further characterise the cell lines. Array CGH confirmed that we had established cisplatin-resistant sublines with distinct genomic patterns but also retained the typical genomic aberrations outlined earlier. No noteworthy genomic alterations were identified which could potentially guide us towards major players in drug resistance, except the focal gain of *NAIP* on chromosome 5 [5]. The overall increase in the number of chromosomal aberrations was common to all resistant sublines and is consistent with the literature [16–18,21,30].

The majority of altered proteins belong to cytoskeletal, nucleic acid binding and chaperone protein families which were detailed among the altered proteins identified by comparative proteomics in different drug resistant cancer cell models [31]. Similar changes in protein expression were reported for cisplatin [32] and etoposide resistant neuroblastoma cell line SH-SY5Y [22]. Subsequently, we further examined the molecular and biological functions of the identified proteins using Ingenuity Pathway Analysis software. By their molecular and cellular function, modulated proteins were mostly classified into proteins involved in 'cell growth and proliferation' and 'cell death and survival'. Comparison of the top five IPA pathways for each cisplatin resistant cell line pair demonstrated that of these five, four top pathways were common for SK-N-ASCis24 (non-MNA) and CHP-212Cis100 (MNA), while KellyCis83 shared one pathway 'Aldosterone Signaling in Epithelial Cells' common to KellyCis83 and CHP-212Cis100 (both MNA). The diversity of pathways involved in the development of cisplatin resistance supports the concept that drug resistant cells can overcome cytotoxic pressure and adapt through establishment of complicated self-defence mechanisms.

The IPA regulator analysis did not predict significant upstream contributors activated by cisplatin in the development of drug resistance in our models. However, the prediction pointed towards proteins involved in the development of resistance to other drugs. The altered expression of beta-tubulin (TUBB), beta-actin (ACTB), vimentin (VIM) and 78 kDa glucose-regulated protein (HSPA5) in all three cisplatin resistant cell lines suggests their potential role in response and cross-resistance to antimicrotubule agents like vincristine [33]. Vimentin was found to be associated with the development of resistance to etoposide in neuroblastoma cell line SH-SY5Y [22]. Vimentin is also considered as a canonical marker of EMT, a cellular re-modelling process in which epithelial cells acquire characteristics of mesenchymal phenotype leading them to dramatically change their shape and display increased motility [8–10,34]. Significant upregulation of VIM and downregulation of cytoskeletal proteins KRT18, KRT8 in SK-N-ASCis24 and CHP212-Cis100 are consistent with changes associated with epithelial-to-mesenchymal transition [8–10]. These two cisplatin resistant cell lines also exhibited a significantly increased invasiveness. The knockdown of cytokeratins, KRT18 and KRT8, alone increased cancer cell motility and invasion without modulating EMT markers [35]. Another member of cytokeratin family, KRT19 was highly correlated with the invasiveness in neuroblastoma cell lines. The study demonstrated significantly lower expression of KRT19 mRNA in stage 4S tumors, which develop metastases, relative to localised primary neuroblastomas, i.e. stage 1 and 2 disease [36]. Hence, the growing body of evidence supports the idea that EMT plays an important role in tumor progression and metastasis as well as the development of chemotherapy resistance [10,37], but it also can be cancer type specific [38].

EMT transcription factors such as the TWIST, ZEB and SNAI families activate the accrual of mesenchymal markers, like VIM and repress epithelial markers such as cytokeratins and E-cadherin during EMT. It is believed that increased production of these transcription factors induces EMT thereby triggering migration and invasion. EMT transcription factors have a significant overlap in their regulation, target genes, and mechanism of action (reviewed in [39,40]). The cross talk between the EMT transcription factors is complicated and not fully understood. Recent data indicate that ZEB factors are downstream of the SNAI and TWIST families in the EMT hierarchy [41]. SNAI1 up-regulates ZEB1 synthesis at both transcriptional and post-transcriptional levels [42–44]. Expression of TWIST1 and SNAI1 is mutually dependent although in different directions depending on the cancer type [44–46]. In this study all drug resistant cell models lost expression of ZEB1 regardless of the expression levels of SNAI1 and TWIST1 and invasiveness of the cell lines. It proposes a common mechanism by which ZEB1 was switched off. The observation also suggests that EMT transcription factors may be affected during the development of cisplatin resistance but to different extents. Of interest is the significant downregulation of SNAI1, TWIST1 and ZEB1, which was registered in the highly invasive drug resistant SK-N-ASCis24 cell line suggesting other cellular players in the invasive mechanism.

The highest scores for actin cytoskeletal signalling, ILK signalling, epithelial adherens junction signalling and remodelling of epithelial adherens junctions in SK-N-ASCis24 are consistent with the observed changes in morphology and invasiveness of this cell line. All of these pathways share common cytoskeletal protein families, such as integrin, actin and myosin, being active players in mesenchymal cell migration [11]. Non-muscle myosin II (MYH9), which was over-expressed by 4-fold in SK-N-ASCis24, is a conventional motor protein known to generate intracellular contractile forces and tension by associating with F-actin and driving cell spreading, migration, cytokinesis, as well as other cellular processes [47–49]. It is considered to be an effector of cell migration and morphogenesis [50]. MYH9 activity is regulated by phosphorylation [13,50] by different kinases including ROCK1 [14]. IPA predicted ROCK1 as a partner in MYH9 containing network, which also contributes to cell invasiveness [12]. An increased expression of ROCK1 was correlated with an increased motility and invasiveness in neuroblastoma [51]. In the present study, we observed an increased invasiveness of SK-N-ASCis24 cell line associated with an increased expression of MYH9 and its network partners rather than ROCK1. This observation can be explained by the mesenchymal phenotype of SK-N-ASCis24 cells acquired during the development of cisplatin resistance. The mesenchymal phenotype does not require elevated levels of ROCK1 for increased cell motility and invasiveness [52].

Our LC–MS data also identified elevated levels of a-Actinins, ACTN1 and ACTN4, in the highly invasive SK-N-ASCis24 cell line. ACTN1 and ACTN4 are members of the spectrin gene superfamily expressed in non-muscle cells [53,54]. These proteins contribute to stabilisation of cell adhesion and regulation of cell shape and cell motility. Recent findings suggest that ACTN1 and ACTN4 play a role in the cell motility and invasion in different types of human cancer including breast [55], bladder [56], colorectal [57], ovarian [58,59] and brain [60]. In contrast, suppression of tumourigenicity by increased expression of ACTN4 was reported in human neuroblastoma cell line SK-N-BE(2) [61].

In this study, SK-N-ASCis24 cell line acquired mesenchymal properties despite the reduced expression of the EMT transcription factors

SNAI1, TWIST1 and ZEB1. The mesenchymal properties included fibroblastoid morphology, increased potential for motility and invasion during the development of chemoresistance, which are prerequisites of EMT [62]. The increased expressions of MYH9 and ACTN4 were observed in the absence of gene amplification, suggesting a potential role for miRNA in their regulation. Our previous study identified a panel of 33 downregulated miRNA in SK-N-ASCis24 [5]. Of the panel, miR-545 and miR-876-3p were predicted to target both genes (Supplementary File S4). Further investigation of the functional relationship between miRNA and proteins is required.

Response to chemotherapy is poor in high risk neuroblastoma, despite treatment with additional drugs such as topotecan and temozolomide, due to the development of drug resistance [3]. Proteomics profiling of a large cohort of neuroblastoma patients would help to identify protein signalling pathways to define the targets for personalised therapy. It will be critical for the development of protein biomarkers of tumour response to chemotherapy or the development of chemoresistance. It would advance both current treatment protocols and selection of patients who may be more likely to benefit from chemotherapy. The drug resistant neuroblastoma cell lines described in this study can greatly complement the clinically identified protein biomarkers in better understanding the efficacy of treatment regimens and drugs.

Thus, the panel of three different cisplatin resistant neuroblastoma cell lines provides a unique and fundamental platform for preclinical studies of the mechanisms underlying the development of drug resistance as well as discovering new drugs and therapeutic targets in neuroblastoma.

Acknowledgements

Work in the authors' laboratory is supported by National Children's Research Centre Grant.

Conflict of interest

The authors declare that they have no conflict of interest.

Appendix: Supplementary material

Supplementary data to this article can be found online at doi:10.1016/j.canlet.2015.05.004.

References

[1] A.M. Davidoff, Neuroblastoma, Semin. Pediatr. Surg. 21 (1) (2012) 2–14.
[2] A.L. Yu, et al., Anti-GD2 antibody with GM-CSF, interleukin-2, and isotretinoin for neuroblastoma, N. Engl. J. Med. 363 (2010) 1324–1334.
[3] W.B. London, et al., Clinical and biologic features predictive of survival after relapse of neuroblastoma: a report from the International Neuroblastoma Risk Group Project, J. Clin. Oncol. 29 (2011) 3286–3292.
[4] Z.H. Siddik, Cisplatin: mode of cytotoxic action and molecular basis of resistance, Oncogene 22 (2003) 7265–7279.
[5] H. Harvey, et al., Modulation of chemotherapeutic drug resistance in neuroblastoma SK-N-AS cells by the neural apoptosis inhibitory protein and miR-520f, Int. J. Cancer 136 (2014) 1579–1588.
[6] P.G. Buckley, et al., Chromosomal and microRNA expression patterns reveal biologically distinct subgroups of 11q- neuroblastoma, Clin. Cancer Res. 16 (11) (2010) 2971–2978.
[7] D.-W. Shen, et al., Cisplatin resistance: a cellular self-defense mechanism resulting from multiple epigenetic and genetic changes, Pharmacol. Rev. 64 (3) (2012) 706–721.
[8] J.M. Lee, et al., The epithelial-mesenchymal transition: new insights in signaling, development, and disease, J. Cell Biol. 172 (7) (2006) 973–981.
[9] J. Lim, J.P. Thiery, Epithelial-mesenchymal transitions: insights from development, Development 139 (19) (2012) 3471–3486.
[10] A. Toll, et al., Epithelial to mesenchymal transition markers are associated with an increased metastatic risk in primary cutaneous squamous cell carcinomas but are attenuated in lymph node metastases, J. Dermatol. Sci. 72 (2) (2013) 93–102.
[11] D.A. Lauffenburger, A.F. Horwitz, Cell migration: a physically integrated molecular process, Cell 84 (3) (1996) 359–369.
[12] N. Rath, M.F. Olson, Rho-associated kinases in tumorigenesis: re-considering ROCK inhibition for cancer therapy, EMBO Rep. 13 (10) (2012) 900–908.
[13] M. Vicente-Manzanares, et al., Non-muscle myosin II takes centre stage in cell adhesion and migration, Nat. Rev. Mol. Cell Biol. 10 (2009) 778–790.
[14] G. Totsukawa, et al., Distinct roles of MLCK and ROCK in the regulation of membrane protrusions and focal adhesion dynamics during cell migration of fibroblasts, J. Cell Biol. 164 (2004) 427–439.
[15] P. Prochazka, et al., Changes in MYCN expression in human neuroblastoma cell lines following cisplatin treatment may not be related to MYCN copy numbers, Oncol. Rep. 29 (6) (2013) 2415–2421.
[16] X. Zheng, et al., Differential effect of long-term drug selection with doxorubicin and vorinostat on neuroblastoma cells with cancer stem cell characteristics, Cell Death Dis. 4 (2013) e740.
[17] M. Flahaut, et al., Molecular cytogenetic characterization of doxorubicin-resistant neuroblastoma cell lines: evidence that acquired multidrug resistance results from a unique large amplification of the 7q21 region, Genes Chromosomes Cancer 45 (2006) 495–508.
[18] R. Kotchetkov, et al., Development of resistance to vincristine and doxorubicin in neuroblastoma alters malignant properties and induces additional karyotype changes: a preclinical model, Int. J. Cancer 104 (2003) 36–43.
[19] M. Michaelis, et al., Onconase induces caspase-independent cell death in chemoresistant neuroblastoma cells, Cancer Lett. 250 (2007) 107–116.
[20] Y. Chen, et al., Micro-RNA-21 regulates the sensitivity to cisplatin in human neuroblastoma cells, J. Pediatr. Surg. 47 (2012) 1797–1805.
[21] F. Baskin, R.N. Rosenberg, V. Dev, Correlation of double-minute chromosomes with unstable multidrug cross-resistance in uptake mutants of neuroblastoma cells, Proc. Natl. Acad. Sci. U.S.A. 78 (1981) 3654–3658.
[22] A. Urban, et al., A proteomic investigation into etoposide chemo-resistance of neuroblastoma cell lines, Proteomics 5 (2005) 796–804.
[23] N. Keshelava, et al., Drug resistance patterns of human neuroblastoma cell lines derived from patients at different phases of therapy drug resistance patterns of human neuroblastoma cell lines derived from patients at different phases of therapy, Cancer Res. 58 (1998) 5396–5405.
[24] S.W. Johnson, et al., Increased platinum-DNA damage tolerance is associated with cisplatin resistance and cross-resistance to various chemotherapeutic agents in unrelated human ovarian cancer cell lines, Cancer Res. 57 (1997) 850–856.
[25] S.W. Johnson, et al., Cross-resistance, cisplatin accumulation, and platinum-DNA adduct formation and removal in cisplatin-sensitive and -resistant human hepatoma cell lines, Exp. Cell Res. 226 (1996) 133–139.
[26] H. Kuroda, et al., Different drug sensitivity in two neuroblastoma cell lines established from the same patient before and after chemotherapy, Int. J. Cancer 47 (1991) 732–737.
[27] R. Bagatell, et al., Phase II study of irinotecan and temozolomide in children with relapsed or refractory neuroblastoma: a Children's Oncology Group study, J. Clin. Oncol. 29 (2) (2011) 208–213.
[28] M. Michaelis, et al., Chemoresistance acquisition induces a global shift of expression of aniogenesis-associated genes and increased pro-angogenic activity in neuroblastoma cells, Mol. Cancer 8 (2009) 80.
[29] M. Michaelis, et al., Chemotherapy-associated angiogenesis in neuroblastoma tumors, Am. J. Pathol. 180 (2012) 1370–1377.
[30] J. Bedrnicek, et al., Characterization of drug-resistant neuroblastoma cell lines by comparative genomic hybridization, Neoplasma 52 (2005) 415–419.
[31] J.T. Zhang, Y. Liu, Use of comparative proteomics to identify potential resistance mechanisms in cancer treatment, Cancer Treat. Rev. 33 (2007) 741–756.
[32] S. D'Aguanno, et al., New insights into neuroblastoma cisplatin resistance: a comparative proteomic and meta-mining investigation, J. Proteome Res. 10 (2011) 416–428.
[33] N.M. Verrills, et al., Proteome analysis of vinca alkaloid response and resistance in acute lymphoblastic leukemia reveals novel cytoskeletal alterations, J. Biol. Chem. 278 (2003) 45082–45093.
[34] A. Satelli, S. Li, Vimentin in cancer and its potential as a molecular target for cancer therapy, Cell. Mol. Life Sci. 68 (18) (2011) 3033–3046.
[35] A.M. Fortier, E. Asselin, M. Cadrin, Keratin 8 and 18 loss in epithelial cancer cells increases collective cell migration and cisplatin sensitivity through claudin1 up-regulation, J. Biol. Chem. 288 (16) (2013) 11555–11571.
[36] M. Nozato, et al., Epithelial-mesenchymal transition-related gene expression as a new prognostic marker for neuroblastoma, Int. J. Oncol. 42 (2013) 134–140.
[37] T. Arumugam, et al., Epithelial to mesenchymal transition contributes to drug resistance in pancreatic cancer, Cancer Res. 69 (2009) 5820–5828.
[38] T.Z. Tan, et al., Epithelial-mesenchymal transition spectrum quantification and its efficacy in deciphering survival and drug responses of cancer patients, EMBO Mol. Med. 6 (10) (2014) 1279–1293.
[39] E. Sánchez-Tilló, et al., EMT-activating transcription factors in cancer: beyond EMT and tumor invasiveness, Cell. Mol. Life Sci. 69 (2012) 3429–3456.
[40] A. Puisieux, T. Brabletz, J. Caramel, Oncogenic roles of EMT-inducing transcription factors, Nat. Cell Biol. 16 (2014) 488–494.
[41] J.H. Taube, et al., Core epithelial-to-mesenchymal transition interactome gene-expression signature is associated with claudin-low and metaplastic breast cancer subtypes, Proc. Natl. Acad. Sci. U.S.A. 107 (35) (2010) 15449–15454.
[42] T. Shirakihara, M. Saitoh, K. Miyazono, Differential regulation of epithelial and mesenchymal markers by δEF1 proteins in epithelial–mesenchymal transition induced by TGF-β, Mol. Biol. Cell 18 (9) (2007) 3533–3544.

[43] S. Guaita, et al., Snail induction of epithelial to mesenchymal transition in tumor cells is accompanied by MUC1 repression and ZEB1 expression, J. Biol. Chem. 277 (42) (2002) 39209–39216.
[44] N. Dave, et al., Functional cooperation between snail1 and twist in the regulation of ZEB1 expression during epithelial to mesenchymal transition, J. Biol. Chem. 286 (14) (2011) 12024–12032.
[45] E. Casas, et al., Snail2 is an essential mediator of twist1-induced epithelial mesenchymal transition and metastasis, Cancer Res. 71 (1) (2011) 245–254.
[46] D.D. Tran, et al., Temporal and spatial cooperation of snail1 and twist1 during epithelial-mesenchymal transition predicts for human breast cancer recurrence, Mol. Cancer Res. 9 (12) (2011) 1644–1657.
[47] M. Guha, M. Zhou, Y.L. Wang, Cortical actin turnover during cytokinesis requires myosin II, Curr. Biol. 15 (2005) 732–736.
[48] K. Murthy, P. Wadsworth, Myosin-II-dependent localization and dynamics of F-actin during cytokinesis, Curr. Biol. 15 (2005) 724–731.
[49] V. Betapudi, Myosin II motor proteins with different functions determine the fate of lamellipodia extension during cell spreading, PLoS ONE 5 (2010) e8560.
[50] R. Aguilar-Cuenca, A. Juanes-García, M. Vicente-Manzanares, Myosin II in mechanotransduction: master and commander of cell migration, morphogenesis, and cancer, Cell. Mol. Life Sci. 71 (2014) 479–492.
[51] J. Lynch, et al., MiRNA-335 suppresses neuroblastoma cell invasiveness by direct targeting of multiple genes from the non-canonical TGF-β signalling pathway, Carcinogenesis 33 (5) (2012) 976–985.
[52] E. Sahai, C.J. Marshall, Differing modes of tumour cell invasion have distinct requirements for Rho/ROCK signalling and extracellular proteolysis, Nat. Cell Biol. 5 (8) (2003) 711–719.
[53] C. Otey, O. Carpen, α- actinin revisited: a fresh look at an old player, Cell Motil. Cytoskeleton 111 (February) (2004) 104–111.
[54] B. Sjöblom, A. Salmazo, K. Djinović-Carugo, Alpha-actinin structure and regulation, Cell. Mol. Life Sci. 65 (17) (2008) 2688–2701.
[55] K.S. Hsu, H.Y. Kao, Alpha-actinin 4 and tumorigenesis of breast cancer, Vitam. Horm. 93 (2013) 323–351.
[56] H. Yoshii, et al., Increased expression of α-actinin-4 is associated with unfavorable pathological features and invasiveness of bladder cancer, Oncol. Rep. 30 (2013) 1073–1080.
[57] K. Honda, et al., Actinin-4 increases cell motility and promotes lymph node metastasis of colorectal cancer, Gastroenterology 128 (2005) 51–62.
[58] S. Yamamoto, et al., Actinin-4 expression in ovarian cancer: a novel prognostic indicator independent of clinical stage and histological type, Mod. Pathol. 20 (2007) 1278–1285.
[59] M. Barbolina V, et al., Motility-related actinin alpha-4 is associated with advanced and metastatic ovarian carcinoma, Lab. Invest. 88 (2008) 602–614.
[60] Q. Quick, O. Skalli, a-Actinin 1 and a-actinin 4: contrasting roles in the survival, motility, and RhoA signaling of astrocytoma cells, Exp. Cell Res. 316 (2010) 1137–1147.
[61] S.N. Nikolopoulos, et al., The human non-muscle alpha-actinin protein encoded by the ACTN4 gene suppresses tumorigenicity of human neuroblastoma cells, Oncogene 19 (2000) 380–386.
[62] A. Singh, J. Settleman, EMT, cancer stem cells and drug resistance: an emerging axis of evil in the war on cancer, Oncogene 29 (34) (2010) 4741–4751.
[63] C.J. Li, R.W. Li, Y.H. Wang, T.H. Elsasser, Pathway analysis identifies perturbation of genetic networks induced by butyrate in a bovine kidney epithelial cell line, Funct. Integr. Genomics 7 (2007) 193–205, doi:10.1007/s10142-006-0043-2.